Journal of Computational Physics 228 (2009) 4549–4567

Contents lists available at ScienceDirect

Journal of Computational Physics

journal homepage: www.elsevier.com/locate/jcp

# Tracking birth of vortex in flows

Jaewook Nam [a], L.E. Scriven [a], Marcio S. Carvalho [b,*]

[a] Coating Process Fundamentals Program, Department of Chemical Engineering and Materials Science, University of Minnesota, Minneapolis, MN 55455, USA
[b] Department of Mechanical Engineering, Pontifícia Universidade Católica do Rio de Janeiro, Rua Marquês de São Vicente 225, Gávea, Rio de Janerio, RJ 22453-900, Brazil

ARTICLE INFO

*Article history:*
Received 30 May 2008
Received in revised form 12 February 2009
Accepted 17 March 2009
Available online 25 March 2009

*Keywords:*
Multiparameter continuation
Automated flow feature tracking
Birth of vortex
Flow topology
Galerkin finite element method
Coating flow

ABSTRACT

In order to avoid undesired effects from vortices in many industrial processes, it is important to know the set of operating parameters at which the flow does not have recirculation. The map of these conditions in the parameter space is called vortex-free operating window. Here, we propose an efficient way to construct such window automatically without expensively checking every possible flow states. The proposed technique is based on tracking a path in the parameter space at which the local kinematic condition at a stagnation point for vortex birth is satisfied. This multiparameter continuation is performed by solving an augmented Navier–Stokes system. In the augmented system, the birth condition and the governing equations was represented in Galerkin's finite element context. We used the proposed method in two important coating flows with free surfaces: single-layer slot coating and forward roll coating.



## 1. Introduction

Vortices in flows are characterized by the rotating motion of material particles around a common center [19]. They can be visualized by examining pathlines constructed from theoretical models or experiments. Numerically or analytically computed streamlines or pathlines illustrate the presence of a vortex by generating multiple-closed loops around a common center. However, streamlines and pathlines are not invariant under a change of frame of reference. For example, a moving sphere in a stationary fluid has closed streamlines varying with time in a laboratory reference; however when the observer moves with the sphere, the flow becomes time-independent and the closed loop streamlines disappear [19]. This example shows that closed streamlines do not guarantee the existence of a vortex: without a proper frame of reference, a vortex can be invisible. In general, vortices show three dimensional spiral structure. But when the pathlines are perpendicular to the axis of rotation, they can be considered plane vortices.

The presence of vortices or recirculations in flows can lead to undesired effects in many industrial processes. In liquid coating, for example, the flow near the region where the liquid meets the moving substrate can develop microscopic gyres that are intense and typically extend across the entire coating bead. These were found in experiments by Coyle [10], Schweizer [23], Sartor [22] and others, as shown in Fig. 1. They tend to centrifuge denser particles, to desorb dissolved gas, to collect and discharge bubbles, to hold formulations long enough for unwanted flocculation or polymerization, and to become nodular along their length and thereby detract from cross-wise coating uniformity. Therefore, the set of operating parameters at which the flow does not present vortices are preferred in order to avoid the problems listed above. It is crucial to map these conditions in the parameter space, and construct the so called vortex-free operating window. The appropriate

* Corresponding author. Tel.: +55 21 3527 1174; +55 21 3527 1165.
*E-mail address:* msc@puc-rio.br (M.S. Carvalho).

0021-9991/$ - see front matter © 2009 Elsevier Inc. All rights reserved.
doi:10.1016/j.jcp.2009.03.017

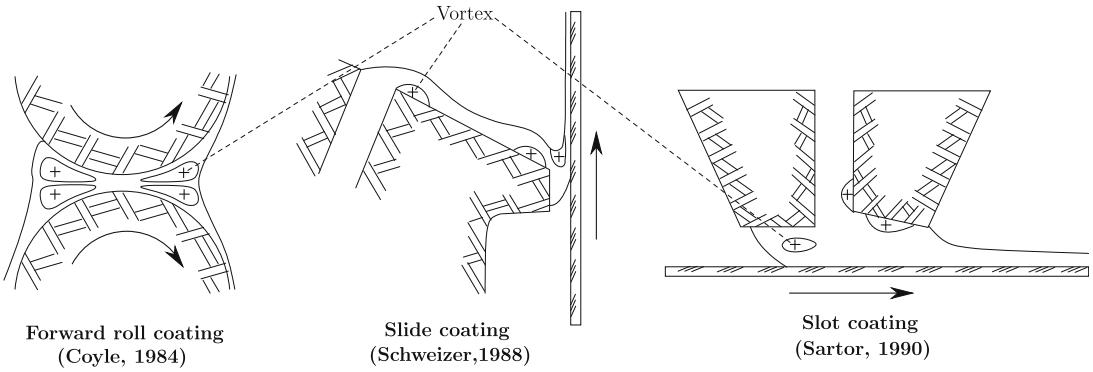


**Fig. 1.** Vortex in coating flows. Roll coating, slide coating, and slot coating flow are illustrated, and possible locations of vortex for each flow system are specified here. Each case the schematic diagram comes from visualization of coating flows [10,23,22].

frame of reference to analyze the presence of undesired vortices in coating flows is the laboratory frame of reference, at which the geometry of the flow does not change with time.

This vortex-free window in the parameter space can be simply obtained by post-processing a large number of steady state solutions at different flow conditions, covering the range of interest in all the flow parameters. This procedure can be called vortex birth capturing and it is extremely expensive, the number of solutions needed to construct the window can easily reach 1000 and post-processing each of these solutions can be very tedious. We propose an alternative efficient way to construct the vortex-free window of a flow.

Historically, vortex analysis is closely related to flow topology analysis [1,20,4]. In two dimensional steady state incompressible flows, the velocity field near a stagnation point may be described by Taylor series expansion around the stagnation point. The characteristics of the expansion terms define the structure of the pathlines in that region. When the stagnation point becomes degenerate, the structure of the pathlines around it changes dramatically. Some of these changes imply the birth of a new vortex.

The event of vortex birth, or death, is signalized by changes in the eigenvalues and eigenvectors of the linear term of the Taylor series expansion of the velocity field around a stagnation point. Three types of vortex birth – inside the flow, from free surface, and from wall – are examined, and local birth conditions are defined in terms of kinematic variables, such as extensional rate, shear rate and vorticity. In the following section we present the vortex birth conditions, which are local flow features evaluated at stagnation points in the flow. In order to determine the set of flow parameters at which a vortex is born (or disappears), we need to find at which flow conditions the local flow feature that defines a vortex birth occurs, i.e. the local flow condition near stagnation points need to be coupled with the global flow parameters.

In this study, we construct the vortex-free window by tracking the global flow conditions at which a recirculation appears (or disappears). This is done by performing a multiparameter continuation to obtain solutions only at the set of conditions at which the local vortex birth condition at stagnation points is satisfied. Therefore, the line (or surface) in the parameter space that defines the boundary of the vortex-free window is constructed automatically. The savings compared to the determination of the window by post-processing a large number of solutions is enormous.

The formulation of the augmented system of equations used in the multiparameter continuation is discussed as well as the solution method used. Three examples are presented, one where a vortex is born from a cusp point inside the flow, a second where it is born from a stationary wall, and a third where it is born from a free surface. All the examples are related to coating flows.

## 2. Vortex birth conditions

With the proper choice of the frame of reference, the description of a fluid particle motion inside a flow can be decomposed into two independent parts – deformation and rotation. In this frame of reference, a flow recirculation is characterized by closed streamlines, and the axis of rotation of the vortex, the *vortex center*, is at rest relative to the observer. As mentioned before, the birth of a vortex is characterized by a dramatic change in the structure of pathlines around an existing stagnation points. In order to identify a vortex birth, characteristics of stagnation points must be analyzed and classified. When a steady state flow system is considered, the fluid particle motion, near a stagnation point, $\mathbf{x}_0$, can be expressed as

$$\frac{D\mathbf{x}}{Dt} = \mathbf{u}(\mathbf{x}) = \mathbf{u}(\mathbf{x}_0) + (\mathbf{x}-\mathbf{x}_0)\cdot\nabla\mathbf{u}(\mathbf{x}_0) + \frac{1}{2}(\mathbf{x}-\mathbf{x}_0)(\mathbf{x}-\mathbf{x}_0) : \nabla\nabla\boldsymbol{u}(\mathbf{x}_0) + \cdots, \tag{1}$$

where $\mathbf{u}(\mathbf{x}_0) = 0$. When $\mathbf{x}$ is close enough to $\mathbf{x}_0$, the characteristic of the flow field depends on the linear term, $\nabla\mathbf{u}(\mathbf{x}_0)$, particularly its eigenvalues and eigenvectors.

Using the irreducible representation of a dyadic, the velocity gradient can be decomposed into a symmetric part, $\boldsymbol{S}$, and an antisymmetric part, $\boldsymbol{A}$:

$$\nabla\mathbf{u} = \underbrace{\frac{1}{2}\left[\nabla\mathbf{u} + (\nabla\mathbf{u})^T\right]}_{\boldsymbol{S}} + \underbrace{\frac{1}{2}\left[\nabla\mathbf{u} - (\nabla\mathbf{u})^T\right]}_{\boldsymbol{A}}. \tag{2}$$

The symmetric part is called the strain rate tensor, which measures the relative motion between fluid particles, i.e. the deformation of a fluid element. The eigenvalues of the symmetric part are

$$\lambda_{\pm}^{S} = \pm\sqrt{-\det\boldsymbol{S}} = \pm\sqrt{\dot{\epsilon}^2 + \dot{\gamma}^2}, \tag{3}$$

where $\dot{\epsilon} = \partial u/\partial x = -\partial v/\partial y$ and $\dot{\gamma} = (\partial v/\partial x + \partial u/\partial y)/2$. Note that $\det\boldsymbol{S} = -(\dot{\epsilon}^2 + \dot{\gamma}^2)$ is always negative and the eigenvalues $\lambda_{\pm}^{S}$ are real. The associated eigenvectors, that represent the flow direction near the stagnation point, are vectors in the flow plane. Along the pathlines, liquid flows toward and away from the stagnation point and $\mathbf{x}_0$ is a saddle point.

The antisymmetric part describes a local solid-body-like rotation around a point and it is sometimes called the *vorticity dyadic*. Its eigenvalues are

$$\lambda_{\pm}^{A} = \pm\sqrt{-\det\boldsymbol{A}} = \pm i\frac{\omega}{2}, \tag{4}$$

where $\omega = (\partial v/\partial x - \partial u/\partial y)$ is called the *vorticity*. Note that $\det\boldsymbol{A} = (\omega/2)^2$ is always positive. Because the eigenvalues are pure imaginary number, pathlines around the stagnation point are concentric circles, and the flow field shows swirling or eddy motion. In this case, the stagnation point is a vortex center.

In order to identify the characteristic of the stagnation point, both parts – symmetric and antisymmetric – should be evaluated together. The eigenvalues (and eigenvectors) can be expressed in terms of the determinant of the symmetric and antisymmetric parts:

$$\lambda_{\pm} = \pm\sqrt{(\dot{\epsilon}^2 + \dot{\gamma}^2) - \left(\frac{\omega}{2}\right)^2} = \pm\sqrt{-\det\nabla\mathbf{u}} = \pm\sqrt{-(\det\boldsymbol{S} + \det\boldsymbol{A})}. \tag{5}$$

When the symmetric part is dominant, i.e. $|\det\boldsymbol{S}| > |\det\boldsymbol{A}|$ or $\dot{\epsilon}^2 + \dot{\gamma}^2 > (\omega/2)^2$, the deformation predominates over the solid body rotation and the stagnation point is a saddle point. When the antisymmetric part is dominant, i.e. $|\det\boldsymbol{S}| < |\det\boldsymbol{A}|$ or $\dot{\epsilon}^2 + \dot{\gamma}^2 < (\omega/2)^2$, the deformation is overwhelmed by the rotation motion and the stagnation point is a vortex center.

The birth of a new vortex can be depicted as the splitting of a stagnation point into two or three stagnation points, including the center of the new vortex, as the flow parameters change. Fig. 2 shows the evolution of the pathlines close to a saddle point (a) and a vortex center (f) as they evolve to give birth to a new vortex – Fig. 2(c) and (d). A vortex can also be born from a cusp point, flow state represented in Fig. 2(h). At the transition states, pathlines shown in (b), (c) and (h), the eigenvalues are equal to zero. According to Brøns [3], these stagnation points are called simple degenerate stagnation points. Therefore, the local condition for the birth (or death) of a vortex is the presence of a degenerate stagnation point, i.e. $(\mathbf{x}_0) = 0$ and $\det\nabla\mathbf{u}(\mathbf{x}_0) = 0$.

Vortex can also be born from flow boundaries, either a gas–liquid interface or a wall. Along them, the associated boundary conditions have to be satisfied together with the velocity expansion around the stagnation point, Eq. (1), which restrict the possible flow patterns.

The flow near a boundary can be described using the tangent and normal directions as the coordinate system. Because the birth of a new vortex from a stagnation point depends only on the kinematics in a region very close to that point, the tangent and normal vectors can be considered constant. In terms of this natural basis set, the position vector is $\mathbf{x} = \mathbf{n}s_n + \mathbf{t}s_t$, and the velocity vector is $\mathbf{u} = \mathbf{n}u_n + \mathbf{t}u_t$. Here $s_t$ and $s_n$ are the arc-length coordinate along the tangential and the normal directions to the interface, and $u_t$ and $u_n$ are the tangential and the normal components of velocity.

Physics along a gas–liquid interface dictates that there is no flow across it, i.e. $u_n = \mathbf{n}\cdot\mathbf{u} = 0$ along the boundary. Only vanishing tangential velocity component, $u_t = 0$, is required to define a stagnation point. Since the no-penetration condition restricts not only the normal velocity component but also its derivative along the boundary, the determinant of velocity gradient is simply

$$\det\nabla\mathbf{u} = -\dot{\epsilon}_s^2, \tag{6}$$

where $\dot{\epsilon}_s = \partial u_t/\partial s_t = -\partial u_n/\partial s_n$. Therefore the vortex birth conditions ($\mathbf{u} = 0$ and $\det\nabla\mathbf{u} = 0$) can be simplified to $u_t = 0$ and $\dot{\epsilon}_s = 0$. For Newtonian liquids, the extensional rate condition, $\dot{\epsilon}_s = 0$, can be expressed as the normal stress condition, $\tau_{tt} = 2\mu\dot{\epsilon}_s = 0$.

The boundary conditions along an impermeable and stationary solid surface are the no-slip and no-penetration conditions: $\mathbf{t}\cdot\mathbf{u} = u_t = 0$ and $\mathbf{n}\cdot\mathbf{u} = u_n = 0$. Because the velocity vanishes along the wall, the Taylor series expansion of the velocity field near a point along the wall, Eq. (1), becomes

$$\frac{D\mathbf{x}}{Dt} = (\mathbf{x}-\mathbf{x}_0)\cdot\nabla\mathbf{u} + \frac{1}{2}(\mathbf{x}-\mathbf{x}_0)(\mathbf{x}-\mathbf{x}_0) : \nabla\nabla\boldsymbol{u} = (s_n - s_{n0})\left[\mathbf{t}(2\dot{\gamma}_s) + \frac{1}{2}(\mathbf{x}-\mathbf{x}_0)\cdot\boldsymbol{Q}\right], \tag{7}$$

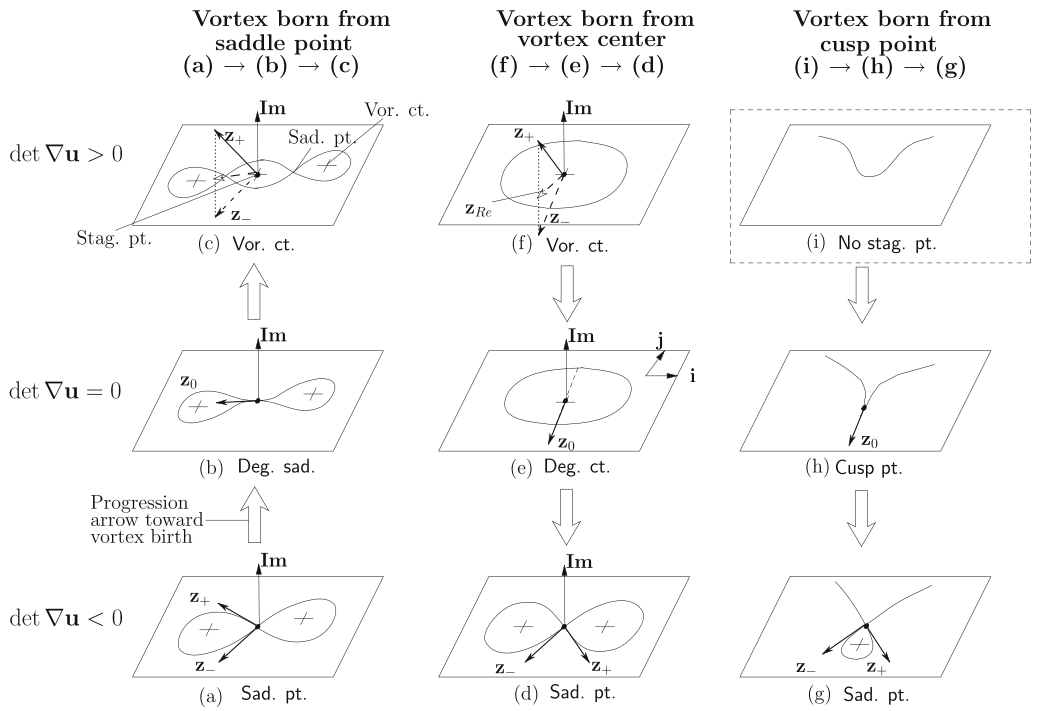


**Fig. 2.** Evolution of eigenvectors at a stagnation point as the determinant of the velocity gradient changes. " Im", "Stag. pt.", "Sad. pt.", "Vor. ct.", "Deg. sd.", "Deg. ct.", and "Cusp pt." stand for imaginary axis, stagnation point, saddle point, vortex center, degenerate saddle point, degenerate vortex center, and cusp point, respectively. There are three possibilities for a vortex birth: born from a saddle point, from a vortex center, and from a cusp point.

where $\mathbf{x} = \mathbf{t}s_t + \mathbf{n}s_n, \dot{\gamma}_s = 1/2(\partial u_t/\partial s_n)$, and $\mathbf{Q}$ is

$$\mathbf{Q} = \mathbf{nn}\left(2\frac{\partial \dot{\gamma}_s}{\partial s_t}\right) + \mathbf{nt}\left(2\frac{\partial \dot{\gamma}_s}{\partial s_n}\right) + \mathbf{tt}\left(-4\frac{\partial \dot{\gamma}_s}{\partial s_t}\right). \tag{8}$$

The quadratic term can be greatly simplified by using the fact that $\partial u_n/\partial s_t = \partial u_t/\partial s_t = 0$. Moreover, as treated in Bakker [1], one can choose unit of time, $\vartheta$, proportional to $(s_n - s_{n0})$ such that the singular character at the wall, caused by the $(s_n - s_{n0})$ term, can be eliminated. Then Eq. (7) becomes

$$\frac{D\mathbf{x}}{Dt^*} = \left[\mathbf{t}(2\dot{\gamma}_s) + \frac{1}{2}(\mathbf{x} - \mathbf{x}_0)\cdot\mathbf{Q}\right], \tag{9}$$

where $t^* = \vartheta t$.

The determinant of the reduced quadratic term, $\mathbf{Q}$, is

$$\det \mathbf{Q} = -8\left(\frac{\partial \dot{\gamma}}{\partial s_t}\right)^2. \tag{10}$$

Therefore, in order to have a degenerate point along a rigid wall, the shear rate and its derivative along the wall need to vanish, i.e. $\dot{\gamma}_s = 0$ and $\partial\dot{\gamma}_s/\partial s_t = 0$. This degenerate point is called *degenerate separation point*. For Newtonian liquids, the conditions can be rewritten as shear stress conditions, $\tau_{tn} = \mu\dot{\gamma}_s = 0$ and $\partial\,\tau_{tn}/\partial s_t = 0$.

In all three scenarios – vortex born inside the flow, from free surface and from solid surfaces, – the vortex birth conditions are expressed in terms of local kinematic variables. They are summarized in Table 1.

**Table 1**
Summary of vortex birth condition in steady two-dimensional incompressible flows.

| Birth type | Vortex birth condition | |
|---|---|---|
| | General fluid | Newtonian fluid |
| Inside flow | $\mathbf{u} = 0$, $\det(\nabla\mathbf{u}) = 0$ | $\mathbf{u} = 0$, $\det(\nabla\mathbf{u}) = 0$ |
| From free surface | $u_t = 0$, $\dot{\epsilon}_s = 0$ | $u_t = 0$, $\tau_{tt} = 0$ |
| From solid surface | $\dot{\gamma}_s = 0$, $\partial\dot{\gamma}_s/\partial s_t = 0$ | $\tau_{tn} = 0$, $\partial\tau_{tn}/\partial s_t = 0$ |

## 3. Automated tracking of vortex birth in flows

The multiparameter continuation described previously was done by augmenting the Navier–Stokes equation by equations that describe the vortex birth condition. The solution of this augmented system was obtained by Galerkin's finite element method. The formulation and solution method for the multiparameter continuation is described in this section.

### 3.1. Navier–Stokes system for viscous free surface flows

The velocity and pressure fields of incompressible pressure fields of two-dimensional, steady state flow of a Newtonian liquid are governed by the continuity and momentum equations:

$$\nabla \cdot \mathbf{u} = 0, \quad \rho \mathbf{u} \cdot \nabla \mathbf{u} = \nabla \cdot \boldsymbol{T}, \tag{11}$$

where $\rho$ is the liquid density and $\boldsymbol{T}$ is stress tensor. For Newtonian liquid, it is given by $-\boldsymbol{T} = -p\boldsymbol{I} + \mu\left[\nabla \mathbf{u} + (\nabla \mathbf{u})^T\right]$, where $p$ is the pressure and $\mu$ is the liquid viscosity.

Boundary conditions are need to solve the Navier–Stokes system. In most case, the flow domain is bounded by inflow and outflow synthetic planes, solid wall and free surface (gas–liquid interface).

At inflow and outflow boundaries, either the velocity components are specified, or a fully developed flow condition is imposed, or the value of pressure is prescribed. The corresponding boundary conditions are:

$$\mathbf{u} = \mathbf{V}_b(\mathbf{x}), \tag{12}$$

$$\mathbf{n}_b \cdot \nabla \mathbf{u} = 0, \tag{13}$$

$$p = p_b. \tag{14}$$

$\mathbf{V}_b(\mathbf{x})$ is the imposed velocity profile, $p_b$ is the imposed pressure, and $\mathbf{n}_b$ is the unit normal vector to the boundary.

At rigid solid walls, the no-slip and no-penetration conditions are imposed:

$$\mathbf{t}_w \cdot \mathbf{u} = V_{\text{wall}}, \quad \mathbf{n}_w \cdot \mathbf{u} = 0, \tag{15}$$

where $V_{\text{wall}}$ is the solid wall velocity, $\mathbf{n}_w$ and $\mathbf{t}_w$ are the unit normal and tangent vectors to the wall.

Along free surfaces, a force balance is imposed and the no-penetration condition (kinematic condition) is used:

$$\mathbf{n}_f \cdot \boldsymbol{T} = \sigma \frac{d\mathbf{t}_f}{ds} - \mathbf{n}_f P_{\text{amb}}, \tag{16}$$

$$\mathbf{n}_f \cdot \mathbf{u} = 0, \tag{17}$$

where $\mathbf{t}_f$ and $\mathbf{n}_f$ are the local unit tangent and unit normal to the free surface, $s$ is the arc-length coordinate along the interface, $\sigma$ is the liquid surface tension and $P_{\text{amb}}$ is the ambient pressure.

Flows with free surface give rise to a *free boundary problem*. The flow domain is unknown *a priori* and it is part of the solution.

To solve a free boundary problem by means of standard techniques for boundary value problems, the set of differential equations and boundary conditions posed in the unknown physical domain have to be transformed to an equivalent set defined in a known, fixed computational domain [18,9]. This transformation is made by a mapping $\mathbf{x} = \mathbf{x}(\xi)$ that connects the two domains. The physical domain is parameterized by the position vector $\mathbf{x} = (x,y)$, and the reference domain, by $\boldsymbol{\xi} = (\xi,\eta)$. The mapping used here is the one described by de Santos [12]. The inverse mapping is governed by a system of elliptic differential equations identical to those encountered in the dilute regime of diffusional transport

$$\nabla \cdot D_\xi(\xi,\eta)\nabla\xi = 0, \quad \nabla \cdot D_\eta(\xi,\eta)\nabla\eta = 0. \tag{18}$$

$D_\xi$ and $D_\eta$ are mesh diffusivities which control the steepness of gradients in the node spacing by adjusting the potentials $\xi$ and $\eta$. Curves of constant $\xi$ and $\eta$ define the boundaries of elements used to describe the domain. The cross point of these curves of sets the position of a node. Boundary conditions are needed to solve the second-order differential Eq. (18). Solid walls and inflow and outflow planes are described by the function that defines their geometry and nodes were distributed along them by a specified stretching function [25]. The location of the free surface is implicitly determined by the kinematic condition, Eq. (17). The discrete version of the mapping equations is generally referred to as mesh generation equations. Detailed procedure and boundary conditions for mesh equations are discussed in de Santos [12] and Benjamin [2].

### 3.2. Solution of the Navier–Stokes system for free surface flow by GFEM

Galerkin finite element method is used to solve the Navier–Stokes system coupled with the mesh generation equation, Eqs. (11) and (18). Each independent variable, velocity, pressure and position, is approximated by a linear combination of a finite number of basis functions [15]:

$$\mathbf{u} = \sum_i \mathbf{U}_i \ \phi^i(\xi,\eta), \tag{19}$$

$$p = \sum_k P_k \ \psi^k(\xi,\eta), \tag{20}$$

$$\mathbf{x} = \sum_i \mathbf{X}_i \ \phi^i(\xi,\eta). \tag{21}$$

$\mathbf{U}_i$,$P_k$ and $\mathbf{X}_i$ are the basis function coefficients, the unknowns of the discretized problem. The velocity and nodal position are represented in terms of Lagrangian bi-quadratic function $\phi^i(\xi,\eta)$, and the pressure in terms of linear discontinuous basis function $\psi^k(\xi,\eta)$.

The weak form of Eqs. (11) and (18) are obtained by multiplying each equation by weighting functions, integrating over the physical domain, and applying the divergence theorem to the appropriate terms with divergence. In Galerkin's method, the weighting and basis functions are the same. The weighted residuals are:

$$\mathbf{R}_m = \int_A \phi^i \rho \mathbf{u} \cdot \nabla \mathbf{u} + \boldsymbol{T} \cdot \nabla \phi^i \, dA - \int_{\partial A} \phi^i \mathbf{n} \cdot \boldsymbol{T} \, ds, \tag{22}$$

$$\mathbf{R}_c = \int_A \psi^k \nabla \cdot \mathbf{u} \, dA, \tag{23}$$

$$\begin{aligned} \mathbf{R}_x^{\xi} &= \int_A D_{\xi} \nabla \xi \cdot \nabla \phi^i \, dA + \int_{\partial A} \phi^i D_{\xi} \mathbf{n} \cdot \nabla \xi \, ds, \\ \mathbf{R}_y^{\eta} &= \int_A D_{\eta} \nabla \eta \cdot \nabla \phi^i \, dA + \int_{\partial A} \phi^i D_{\eta} \mathbf{n} \cdot \nabla \eta \, ds, \end{aligned} \tag{24}$$

where $A$ is the flow domain and $\partial A$ is the domain boundary and $s$ is arc-length coordinate along the boundary. The superscripts, $m$,$c$ and $x$, denote momentum, continuity and mesh residuals, respectively. Essential boundary conditions were imposed by replacing the corresponding weighted residual equation with the desired velocity or node specification. Natural boundary conditions were applied through the boundary integrals in Eqs. (22) and (24).

In sum, the Galerkin finite element method reduces the Navier–Stokes and mesh generation differential equations to a set of non-linear algebraic equations on the basis functions coefficients.

$$\mathbf{R}(\mathbf{z},\lambda) = \mathbf{0}, \tag{25}$$

where $\mathbf{z}$ is the solution vector which consist of velocity $\mathbf{u}$, pressure $P$ and position $\mathbf{x}$, and $\lambda$ is a vector that contains the $M$ parameters on which the system depends. Eq. (25) is solved iteratively by Newton's method:

$$\begin{aligned} \boldsymbol{J}^{(i)}(\mathbf{z}^{(i)},\lambda)\delta\mathbf{z}^{(i)} &= -\mathbf{R}^{(i)}(\mathbf{z}^{(i)},\lambda), \\ \mathbf{z}^{(i+1)} &= \mathbf{z}^{(i)} + \delta\mathbf{z}^{(i)}, \end{aligned} \tag{26}$$

the index $i$ and $i+1$ indicate the current and next Newton's step. $\boldsymbol{J}^{(i)} \equiv \partial\mathbf{R}^{(i)}/\partial\mathbf{z}^{(i)}$ is the Jacobian matrix. The iteration continues until $\|\mathbf{R}^{(i)}\|_2 < \epsilon$. Here we choose $10^{-8}$ as $\epsilon$.

### 3.3. Tracking the vortex birth condition

Following the procedure described in the previous section, one can get a flow state at specified set of flow parameters.

In order to use Galerkin's finite element method to solve the augmented system, the conditions described in Table 1 need to be written in terms of the finite element basis functions. For a vortex birth inside the flow, the discretized birth conditions are:

$$\begin{aligned} u(x^*,y^*) &= \sum_i U_i \phi_i(x^*,y^*) = 0, \\ v(x^*,y^*) &= \sum_i V_i \phi_i(x^*,y^*) = 0, \\ \det \nabla\mathbf{u}(x^*,y^*) &= \frac{\partial u}{\partial x}(x^*,y^*)\frac{\partial v}{\partial y}(x^*,y^*) - \frac{\partial v}{\partial x}(x^*,y^*)\frac{\partial u}{\partial y}(x^*,y^*) \\ &= \left(\sum_i U_i \frac{\partial \phi_i}{\partial x}(x^*,y^*)\right)\left(\sum_i V_i \frac{\partial \phi_i}{\partial y}(x^*,y^*)\right) - \left(\sum_i V_i \frac{\partial \phi_i}{\partial x}(x^*,y^*)\right)\left(\sum_i U_i \frac{\partial \phi_i}{\partial y}(x^*,y^*)\right) = 0, \end{aligned} \tag{27}$$

where $u$ and $v$ are the velocity component in $x$ and $y$ direction, $U_i$ and $V_i$ are the nodal value of velocity components, and $(x^*,y^*)$ stands for the coordinate of the vortex birth point.

The discretized conditions for a vortex birth from free surface are:

$$\begin{aligned}
u_t(x^*,y^*) &= (\mathbf{t}\cdot\mathbf{u})(x^*,y^*)\\
&= \left(t_x\sum_i U_i\phi_i\right)\Big|_{(x^*,y^*)} + \left(t_y\sum_i V_i\phi_i\right)\Big|_{(x^*,y^*)} = 0,\\
\tau_{tt}(x^*,y^*) &= (\mathbf{tt}:\boldsymbol{T})(x^*,y^*)\\
&= \left[t_xt_x\,\mu\left(2\sum_i U_i\frac{\partial\phi_i}{\partial x}\right) + t_xt_y\mu\left(\sum_i U_i\frac{\partial\phi_i}{\partial y}\sum_i V_i\frac{\partial\phi_i}{\partial x}\right)\right.\\
&\quad \left. + t_yt_x\mu\left(\sum_i U_i\frac{\partial\phi_i}{\partial y}\sum_i V_i\frac{\partial\phi_i}{\partial x}\right) + t_yt_y\mu\left(2\sum_i V_i\frac{\partial\phi_i}{\partial y}\right)\right]\Big|_{(x^*,y^*)} = 0,
\end{aligned} \tag{28}$$

where $\mathbf{t}$ is the tangent vector to the free surface.

The birth conditions from a solid surface are related to the shear stress and its derivative with respect to the arc-length coordinate, $\tau_{tn} = 0$ and $\partial\tau_{tn}/\partial s_t = 0$. When quadratic basis functions are used to expand the velocity field, the stress is linear inside each element and its derivative is constant. Therefore, it is impossible to locate a point inside an element from which a vortex is born. Instead of this condition, we use an "alleviated" version. The vortex birth (or death) condition at solid surface can be interpreted as two (or more) adjacent stagnation points that split (or collapse) from (into) a single degenerate stagnation point. Therefore, the birth condition at a solid wall can be approximated as

$$\frac{\partial\tau_{tn}}{\partial s_t}(s_t^*) \approx \frac{\tau_{tn}(s_t^*+\delta s_t) - \tau_{tn}(s_t^*)}{\delta s_t} = 0, \tag{29}$$

where $s_t^*$ is the arc-length coordinate along the solid surface at the vortex birth point, $\delta s_t$ is the distance between the two separated but close stagnation points. Therefore, vortex birth is approximated as the condition at which adjacent stagnation points are located close enough to each other. Using this fact, the vortex birth condition for Newtonian liquid becomes,

$$\begin{aligned}
\tau_{tn}(s_t^*) &= (\mathbf{tn}:\boldsymbol{T})(s_t^*)\\
&= \left[t_xn_x\mu\left(2\sum_i U_i\frac{\partial\phi_i}{\partial x}\right) + t_xn_y\mu\left(\sum_i U_i\frac{\partial\phi_i}{\partial y}\sum_i V_i\frac{\partial\phi_i}{\partial x}\right)\right.\\
&\quad \left. + t_yn_x\mu\left(\sum_i U_i\frac{\partial\phi_i}{\partial y}\sum_i V_i\frac{\partial\phi_i}{\partial x}\right) + t_yn_y\mu\left(2\sum_i V_i\frac{\partial\phi_i}{\partial y}\right)\right]\Big|_{(s_t=s_t^*)} = 0\\
\tau_{tn}(s_t^*+\delta s_t) &= (\mathbf{tn}\cdot\boldsymbol{T})(s_t^*+\delta s_t) = 0,
\end{aligned} \tag{30}$$

where $\mathbf{t} = t_x\mathbf{i} + t_y\,\mathbf{j}$ and $\mathbf{n} = n_x\mathbf{i} + n_y\mathbf{j}$ are the tangent and normal vector to the solid surface. This condition is the one used by Yeckel and Scriven [27], and Yeckel [28] to describe the birth of a vortex inside the feed slot of a slot coating flow. In this study, we set $\delta s_t$ to be equal to the size of the largest element along the solid wall boundary. It is impossible to have more than one root of the shear stress distribution along a single element because of the quadratic basis function used for the velocity field.

### 3.4. Augmented Navier–Stokes system

The augmented system of algebraic equations consists of the algebraic equations that relate the finite element coefficients of the unknown fields and the conditions of vortex birth. The set of unknowns is also augmented by the number of algebraic equations that define the vortex birth condition, Three in the case of vortex birth inside the flow – Eqs. (27), and two in the case of vortex birth at a free surface or solid wall – Eqs. (28) or (30). The extra unknowns are the position of the stagnation point at which a vortex is born from and one of the flow parameters $\lambda_1$ that is not fixed. Actually, the solution of the augmented system will give the value of this parameter at which the vortex birth occurs. For a birth inside a flow, two coordinates $(x^*,y^*)$ are required to locate the stagnation point. For a birth attached to a flow boundary, either solid surface or free surface, only one coordinate is enough to locate the birth point.

The augmented system of equation can be

$$\begin{cases}\mathbf{R}(\mathbf{z},\boldsymbol{\lambda},\mathbf{p}) = 0,\\ \mathbf{A}(\mathbf{z},\boldsymbol{\lambda},\mathbf{p}) = 0,\end{cases} \tag{31}$$

where $\mathbf{z}$ and $\boldsymbol{\lambda}$ are the vectors that contain the finite element coefficients and fixed flow parameters, as defined in Eq. (26), and $\mathbf{p}$ is a vector that contains the extra set of unknowns of the augmented problem, e.g. $\mathbf{p} = (\mathbf{x}^*,\lambda_1)$. $\mathbf{A}$ is the set of algebraic equations that defines the vortex birth condition.

This non-linear system is solved by Newton's method, which requires the evaluation of the Jacobian matrix of the system:

$$\left[\begin{array}{c|c} \frac{\partial \mathbf{R}}{\partial \mathbf{z}} & \frac{\partial \mathbf{R}}{\partial \mathbf{p}} \\ \hline \frac{\partial \mathbf{A}}{\partial \mathbf{z}} & \frac{\partial \mathbf{A}}{\partial \mathbf{p}} \end{array}\right] \left[\begin{array}{c} \delta \mathbf{z} \\ \hline \delta \mathbf{p} \end{array}\right] = - \left[\begin{array}{c} \mathbf{R} \\ \hline \mathbf{A} \end{array}\right], \tag{32}$$

where $\partial \mathbf{R}/\partial \mathbf{p}$ are the sensitivity of the residual equations to the extra unknowns and $\partial \mathbf{A}/\partial \mathbf{p}$ are the sensitivity of the vortex birth conditions to the flow field (finite element coefficients) and extra unknowns, respectively. $\partial \mathbf{R}/\partial \mathbf{z}$ is the Jacobian matrix of the original problem.

Because the new three blocks are usually small sub-matrices that are generally densely populated, the fill structure of the new matrix is that of an arrow head, which destroys the benefit of most direct sparse linear solver [21]. This difficulty can be alleviated by employing the bordering algorithm [17], or block elimination on the solution of the linear system at each Newton iteration. The basic idea is to decompose the matrix–vector equations and solve them sequentially.

To construct the augmented Jacobian matrix, we need to evaluate these three new blocks. The sensitivity of the vortex birth conditions to the finite element coefficients $\partial \mathbf{A}/\partial \mathbf{z}$ is easily calculated, because the velocity and pressure field explicitly appear in the algebraic equations that define a vortex birth.

The derivative of the Navier–Stokes residual with respect to the auxiliary parameters $\mathbf{p}$ is not readily available. When a given parameter explicitly appears in the Navier–Stokes equation, the evaluation of the sensitivity is straight forward. For example, if the parameter $\lambda_1$ that belongs to $\mathbf{p}$ is the Reynolds number ($\lambda_1 = N_{Re}$), analytical entries for $\partial \mathbf{R}/\partial N_{Re}$ can be easily computed. If the set of equations depends on the parameter implicitly, for example, if the free parameter is a geometrical parameter that defines a flow boundary, it is impossible to construct ($\partial \mathbf{R}/\partial \lambda_1$) analytically. However, it can be easily approximated by a finite difference quotient, as the central difference secant approximation to the tangent [21]:

$$\frac{\partial \mathbf{R}}{\partial \lambda_1} \approx \frac{\mathbf{R}(\lambda_1 + \epsilon_\lambda) - \mathbf{R}(\lambda_1 - \epsilon_\lambda)}{2\epsilon_\lambda}. \tag{33}$$

Here $\epsilon_\lambda$ is a small number, say, $\epsilon_\lambda = \lambda_1 \times 10^{-6}$, or $10^{-6}$ when $\lambda_1$ is zero.

The derivative of the augment equations with respect to the extra unknowns $\partial \mathbf{A}/\partial \mathbf{p}$ can be a problem. The augment equations used here are based on local flow features near stagnation point. In finite element context, the equations that describe the conditions for vortex birth are evaluated inside or along the element which contains the stagnation point "under surveillance". However, the entire flow field is affected by changes of the flow parameter $\lambda_1$. Therefore, the dependence of the augment equations on the unknown flow parameter $\lambda_1$ and on the location of the stagnation point $(x^*, y^*)$ is not explicit, and the evaluation of the sensitivity of augment equations with respect to extra unknown vector $\partial \mathbf{A}/\partial \mathbf{p}$ is not straight forward to compute.

For example, the determinant of velocity gradient during $i$th Newton's step can be represented as $(\det \nabla \mathbf{u})^{(i)}(\mathbf{z}^{(i)}(\lambda_1), x^{*,(i)}, y^{*,(i)})$. The first argument indicates the effect of changes in the parameter $\lambda_1$ on the solution vector – the indirect dependence. The second and third arguments indicate the direct dependence on the $i$th step vortex birth position, $(x^{*,(i)}, y^{*,(i)})$. In this case, the augmented Jacobian entries corresponding to extra unknowns can be approximated as

$$\frac{\partial (\det \nabla \mathbf{u})^{(i)}}{\partial \lambda_1}(\mathbf{z}^{(i)}(\lambda_1), x^{*,(i)}, y^{*,(i)}) \approx \frac{(\det \nabla \mathbf{u})^{(i)}(\mathbf{z}^{(i)}(\lambda_1 + \epsilon_\lambda), x^{*,(i)}, y^{*,(i)}) - (\det \nabla \mathbf{u})^{(i)}(\mathbf{z}^{(i)}(\lambda_1), x^{*,(i)}, y^{*,(i)})}{\epsilon_\lambda}, \tag{34}$$

$$\frac{\partial (\det \nabla \mathbf{u})^{(i)}}{\partial x^*}(\mathbf{z}^{(i)}(\lambda_1), x^{*,(i)}, y^{*,(i)}) \approx \frac{(\det \nabla \mathbf{u})^{(i)}(\mathbf{z}^{(i)}(\lambda_1), x^{*,(i)} + \epsilon_x, y^{*,(i)}) - (\det \nabla \mathbf{u})^{(i)}(\mathbf{z}^{(i)}(\lambda_1), x^{*,(i)}, y^{*,(i)})}{\epsilon_x}, \tag{35}$$

$$\frac{\partial (\det \nabla \mathbf{u})^{(i)}}{\partial y^*}(\mathbf{z}^{(i)}(\lambda_1), x^{*,(i)}, y^{*,(i)}) \approx \frac{(\det \nabla \mathbf{u})^{(i)}(\mathbf{z}^{(i)}(\lambda_1), x^{*,(i)}, y^{*,(i)} + \epsilon_y) - (\det \nabla \mathbf{u})^{(i)}(\mathbf{z}^{(i)}(\lambda_1), x^{*,(i)}, y^{*,(i)})}{\epsilon_y}, \tag{36}$$

where $\epsilon_x$ and $\epsilon_y$ are $10^{-6}$ in this study.

The evaluation of Eqs. (35) and (36) are straight forward: each term in numerator are just evaluated at different positions at the given parameter $\lambda_1$. However, Eq. (34) needs a *special* treatment because it is not trivial to obtain $\mathbf{z}^{(i)}(\lambda_1 + \epsilon_\lambda)$ which means the $i$th step solution vector with the perturbed parameter. Once you solve the system at $\lambda_1 + \epsilon_\lambda$, the resulting solution vector does not belonged to $i$th Newton step of the system at $\lambda_1$ anymore!

A simple way to approximate $\mathbf{z}^{(i)}(\lambda_1 + \epsilon_\lambda)$ is to use Taylor series expansion around $\lambda_1$:

$$\mathbf{z}^{(i)}(\lambda_1 + \epsilon_\lambda) = \mathbf{z}^{(i)}(\lambda_1) + \epsilon_\lambda \frac{\partial \mathbf{z}^{(i)}(\lambda_1)}{\partial \lambda_1} + \underbrace{\epsilon_{\lambda_1}^2 \frac{\partial^2 \mathbf{z}^{(i)}(\lambda_1)}{\partial \lambda_1^2} + \cdots}_{\text{Higher order term}} \tag{37}$$

Because $\epsilon_\lambda$ is a small number, higher order term can be neglected. $\mathbf{z}^{(i)}(\lambda_1)$ is already known by solving Eq. (26) of $(i-1)$th step. $\partial \mathbf{z}^{(i)}(\lambda_1)/\partial \lambda_1$ can be obtained by

$$\boldsymbol{J}^{(i)}(\mathbf{z}^{(i)}(\lambda_1)) \frac{\partial \mathbf{z}^{(i)}(\lambda_1)}{\partial \lambda_1} = -\frac{\partial \mathbf{R}^{(i)}}{\partial \lambda_1}(\mathbf{z}^{(i)}(\lambda_1)). \tag{38}$$

The Jacobian matrix is the same as Eq. (26) and the right hand side can be approximated as in Eq. (33). This equation will appear in the predictor step of the continuation procedure in direct tracking algorithm – the result can be reused, improving the efficiency of the method.

### 3.5. Direct tracking algorithm

Using the augmented Navier–Stokes system and the solution strategy discussed on Section 3.4, one can perform *direct tracking of vortex birth*: an automated vortex birth tracking algorithm. Multiparameter continuation is the heart of this algorithm.

The basic scheme is shown in Fig. 3. $\alpha$ and $\beta$ stand for chosen operating or design parameters from the parameter space that define a plane at which a vortex-free window will be constructed. This plane is a cut on a multi-dimensional parameter space. Specifically, $\alpha$ is the parameter which will remain part of the solution of the augmented Navier–Stokes system, and $\beta$ is the control variable, which is changed by a user-defined rule during continuation.

Step **I** in Fig. 3 represents the evaluation of a flow state at a fixed set of parameters $\alpha$ and $\beta$ which is close enough to a vortex birth state. Either solution, with or without vortex, will work but "close enough" means it should provide a good initial guess for Step **II**.

Step **II** corresponds to the search of the first vortex birth state at a fixed value of $\beta$, that is, finding the critical value of $\alpha$ at which the vortex birth condition is satisfied at a fixed $\beta$. For solving the augmented Navier–Stokes system, as explained in Section 3.4, Newton's method is used until the $\mathscr{L}_2$ norm of the augmented residual, $\|\mathbf{R}^A(\mathbf{z}^A)\|_2$, is less than $10^{-8}$. This step gives the starting point of the direct tracking procedure.

Steps **III** to **V** is the *multiparameter continuation*: increase or decrease $\beta$ based on a specified rule, and find the critical value of $\alpha$ at fixed $\beta$ at which a vortex is born. Cycling process through **III** to **V** will continue to construct the boundary of the vortex-free window.

Step **III** corresponds to changing $\beta$ based on a given rule. One can apply an adaptive step-size control strategy in this step based on the result from the predictor or corrector step during the continuation, as described in Seydel [24]. In this study, we simply used $\beta_{(i+1)} = \beta_{(i)} + \delta\beta$, where subscript stands for the number of continuation step and $\delta\beta$ is a given step size that depends on the flow.

Step **IV** is the predictor step in the continuation which generate the "good" initial guess for the corrector step. According to Seydel [24], there are two types of predictor: tangent predictor or polynomial extrapolation. In this study, we use the tangent predictor type. Because the control variable is $\beta$, the equation used to evaluate the tangent, $\partial\mathbf{z}^A/\partial\beta$, is,

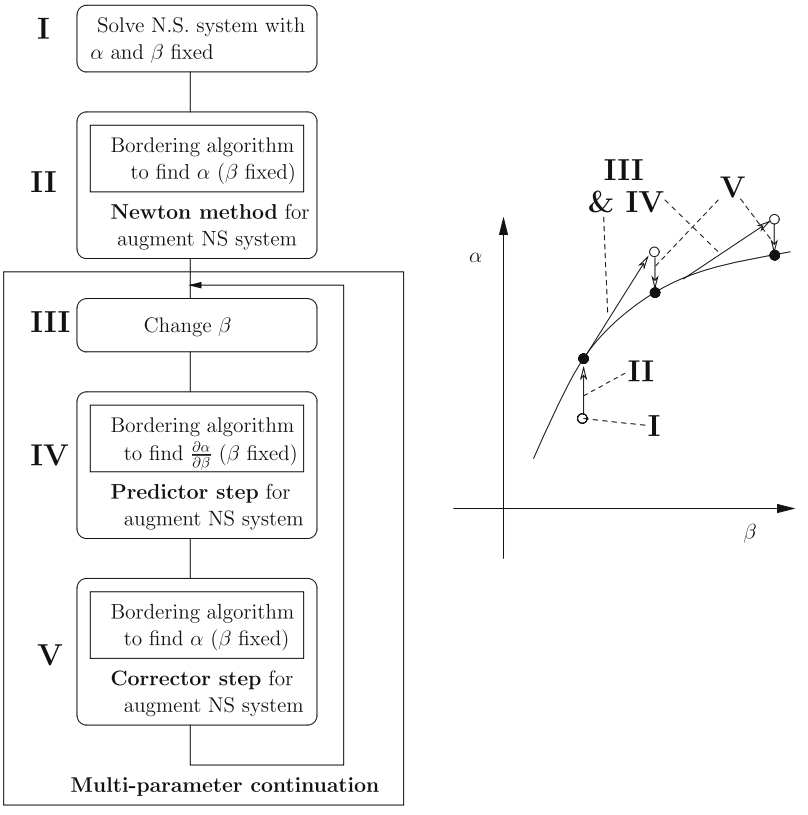


**Fig. 3.** Schematic procedure of direct tracking algorithm. $\alpha$ and $\beta$ are the chosen operating or design parameter and NS stands for Navier–Stokes system.

$$\left[\begin{array}{c|c} \boldsymbol{J} & \frac{\partial \mathbf{R}}{\partial \mathbf{p}} \\ \hline \frac{\partial \mathbf{A}}{\partial \mathbf{z}} & \frac{\partial \mathbf{A}}{\partial \mathbf{p}} \end{array}\right] \left[\begin{array}{c} \frac{\partial \mathbf{z}}{\partial \beta} \\ \hline \frac{\partial \mathbf{p}}{\partial \beta} \end{array}\right] = - \left[\begin{array}{c} \frac{\partial \mathbf{R}}{\partial \beta} \\ \hline \frac{\partial \mathbf{A}}{\partial \beta} \end{array}\right] \tag{39}$$

Note that the Jacobian of the augmented system is the same as Eq. (32). If $\beta$ explicitly appears on $\mathbf{A}$, one can use an analytic expansion for $\partial\mathbf{A}/\partial\beta$. If not, one can use the same technique used in Eq. (33) to approximate the derivative by a secant. The other blocks were already discussed in Section 3.4. Using the tangent predictor, an initial guess for the corrector iterations is computed by $\bar{\mathbf{z}}^A_{(i+i)} = \mathbf{z}^A_{(i)} + \delta\beta(\partial\mathbf{z}^A_{(i)}/\partial\beta)$, where $\bar{\mathbf{z}}^A_{(i+i)}$ stands for the initial guess for $(i+1)$th continuation step.

Step **V** is the corrector step. The type of corrector depends on how the curve is parameterized. The parameter used for describing the curve is called *the curve parameter* [24]. What we called first-order or natural continuation is that the curve parameter is the control variable, $\beta$. In this case, Jacobian matrix and the residual vector of corrector step are basically the same as augmented Navier–Stokes system, Eq. (32). Step **V** is similar to Step **II**. To avoid singular points on the branch, as turning points, the curve need to be parameterized properly. Typically, pseudo arc-length parameterization is used: add one more equation, arc-length definition, to augment the residual, and one more parameter, arc-length $s$, to the auxiliary parameter vector. Detailed methods about pseudo arc-length continuation are described in Chain [8]. In this study, we use first-order continuation to construct the vortex birth curve of a given flow system.

## 4. Examples

As mentioned before, vortex in flows can cause problems in industrial process, especially continuous coating of substrates. In this study, we choose two coating systems, slot coating and forward roll coating, as examples of automated tracking of vortex birth. By using the vortex birth tracking, we were able to create vortex-free windows which can be used as guide-lines for operating conditions or design parameters in a very efficient way.

### 4.1. Single-layer slot coating

Single-layer slot coating is a high-precision coating method used to deposit a thin liquid film onto a moving substrate. It is classified as a pre-metered coating method: the coated thickness is directly controlled by the flow rate and web speed and independent of other process variables. However, the liquid flow in the application region, so called the *coating bead*, is strongly affected by operating parameters, liquid properties, and design parameters; such as web speed, surface tension, and geometry of the coating die. Extensive research has been done to find the region in the parameter space of acceptable coating quality [16,22,14,6]. But here, we focused on the vortex birth inside coating bead and tracked it using direct tracking.

In this study, the coating liquid is considered Newtonian. The geometry of the flow and the boundary conditions are summarized in Fig. 4(a).

The geometric parameters of the die shape considered here are the upstream gap $h_{ug}$, the downstream gap at the upstream corner $h_{dg,u}$ and the downstream gap at the downstream corner $h_{dg,d}$ and the length of the upstream and downstream lips $L_u$ and $L_d$, as indicated in Fig. 4(b). Note that the downstream die-lip angle $\theta$ is defined in terms of these variables

$$\theta = \tan^{-1}\left(\frac{h_{dg,u} - h_{dg,d}}{L_d}\right). \tag{40}$$

Operating and geometric parameters and their values at a base case used in this study are summarized in Table 2.

The finite element mesh used to computed the results presented here is shown in Fig. 4(c). It consisted of 920 elements and 18,300 degrees of freedom.

In slot coating operation, as shown in Fig. 1, recirculation usually occurs in two different regions of the flow; under the upstream die lip and under the downstream die lip. In the first case, the turn around flow with zero net flow rate may lead to a vortex formation. Under the downstream lip, recirculation attached to the wall may appear if the adverse pressure gradient is high enough.

#### 4.1.1. Tracking cusp point under upstream die lip

In typical slot coating operation, vacuum pressure is applied at the upstream meniscus of a slot coater in order to move the meniscus away from the feed slot and to obtain thin coatings [22]. The net flow rate under the upstream die lip is zero. The liquid flows upstream because of the pressure difference and flow upstream dragged by the moving web. The length of the die lip that is wetted by the liquid is a function of the imposed pressure difference. The lower the upstream pressure, the longer is the upstream coating bead. If the upstream bead is short the flow turns around without forming a vortex. If the upstream bead is too long, a vortex is formed inside the flow. This transition between these two states implies a cusp point formation as sketched in Fig. 5.

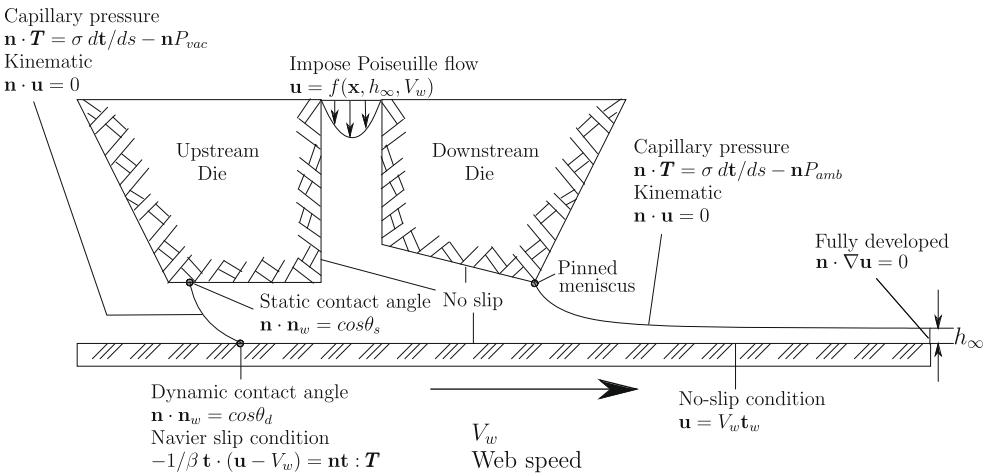


(a) Sketch of flow domain and boundary conditions used for a single-layer slot coating flow.

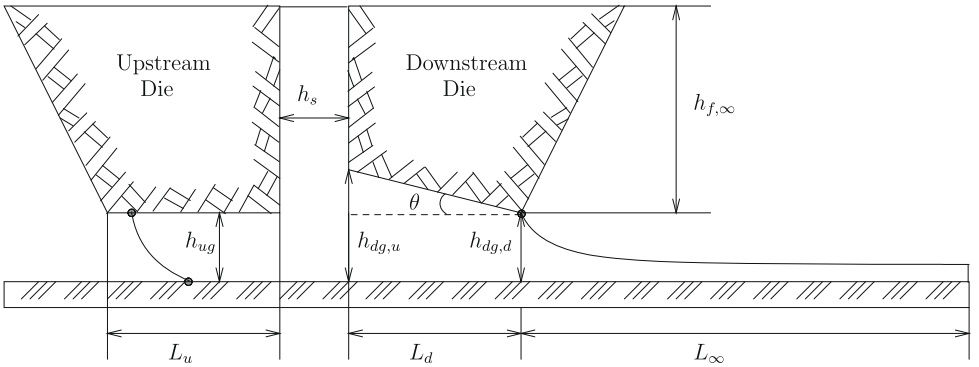


(b) Geometry parameters used for a single-layer slot coating flow.

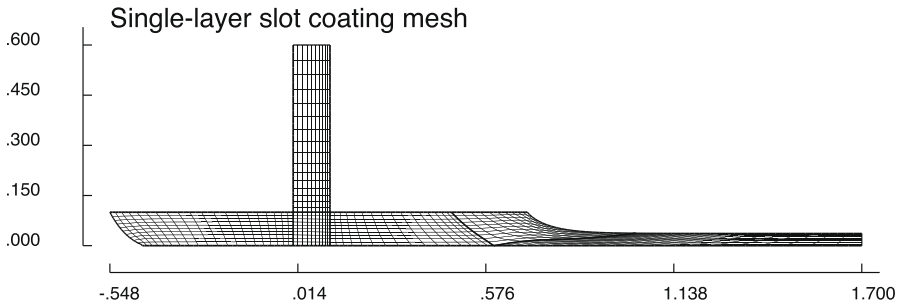


(c) Mesh used to solve the governing equations by G/FEM 920 elements and 18300 unknown coefficients of the finite element basis functions are used to discretize the system.

**Fig. 4.** Single-layer slot coating: boundary condition, design parameter and mesh.

In this study, we focus on two parameters which affect the length of the upstream coating bead and consequently the presence of a vortex: flow rate and vacuum pressure. High flow rates lead to long coating beads. We choose vacuum pressure $P_{\text{vac}}$ as the control variable for the continuation method, and flow rate $q$ as the auxiliary parameter for the augmented Navier–Stokes system. Augmented residuals are Eqs. (27), and the additional auxiliary parameters for the augment

**Table 2**
Parameters used in single-layer slot coating.

| Name | Unit | Base case |
|---|---|---|
| *Operating parameters* | | |
| Film thickness ($h_\infty$) | mm | 0.05 |
| Web speed ($V_w$) | m/s | 1 |
| Vacuum pressure ($P_{vac}$) | Pa | −1000 |
| Ambient pressure ($P_{amb}$) | Pa | 0 |
| Surface tension ($\sigma$) | dyne/cm | 61 |
| Viscosity ($\mu$) | MPa · s | 2.3 |
| Density ($\mu$) | g/cm$^3$ | 1.2 |
| Dynamic contact angle ($\theta_d$) | deg. | 128 |
| Static contact angle ($\theta_s$) | deg. | 62 |
| *Model geometry parameters* | | |
| Upstream gap height ($h_{ug}$) | mm | 0.1 |
| Downstream gap height at downstream corner ($h_{dg,d}$) | mm | 0.1 |
| Downstream gap height at upstream corner ($h_{dg,u}$) | mm | 0.1 |
| Downstream lip angle ($\theta$) | deg. | 0 |
| Upstream lip length ($L_u$) | mm | 0.6 |
| Downstream lip length ($L_d$) | mm | 0.6 |
| Fully developed length ($L_\infty$) | mm | 1.1 |
| Feed slot width ($h_s$) | mm | 0.1 |
| Feed slot height ($h_{f,\infty}$) | mm | 0.6 |

Dimensionless variables used in vortex-free window

| Name | Definition |
|---|---|
| Dimensionless flow rate ($q^*$) | $\frac{h_\infty}{h_{ug}}$ |
| Dimensionless vacuum ($P^*_{vac}$) | $\frac{P_{vac}}{\frac{\mu V_w}{h_{ug}}}$ |

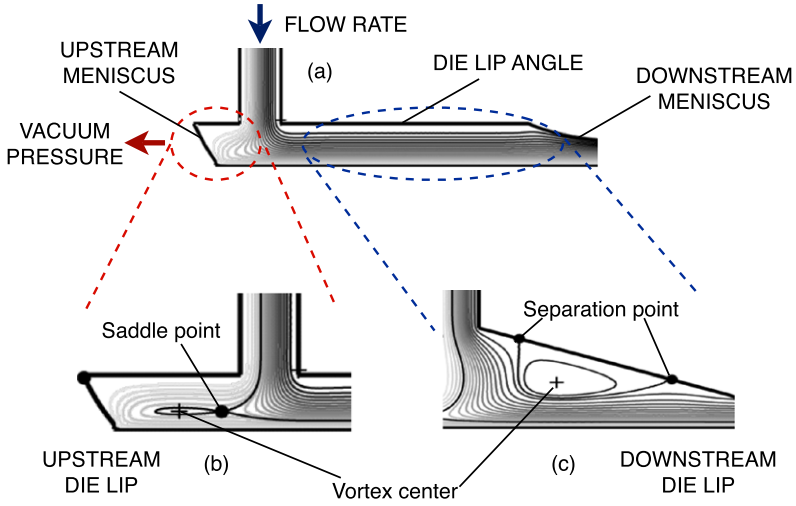


**Fig. 5.** Possible vortices inside slot coating and the flow parameters which can induce vortex birth. Three figures, (a)-(c), are streamline plots of steady slot coating flows at different conditions (a) represents slot coating operation without vortex, and (b) and (c) represent upstream and downstream die lip region with vortices. Note that vortex inside upstream coating bead attached to saddle point, and vortex under downstream die lip is enclosed by a separating streamline, attached to the die lip.

Navier–Stokes system are the two coordinates $x$ and $y$ of the cusp point and the flow rate $q$. The remaining flow parameters are the ones listed in Table 2.

The path of solution of the augmented Navier–Stokes system in the plane of dimensionless flow rate $q^* = q/(V_w h_{ug})$ and dimensionless vacuum pressure $P^*_{vac} = P_{vac}/(\mu V_w/h_{ug})$ is presented in Fig. 6. All the flow states over the constructed path present a cusp point, as illustrated in insert (a) of the figure, that marks the onset of a vortex birth. As discussed before, this curve is the boundary of the vortex-free window in this plane of parameters. For the purpose of illustration, we computed solutions at a set of parameters away from the constructed path. These flow states are illustrated in inserts (b) and (c) of the figure. Flow state (b) was obtained at a set of parameters above the computed path; the presence of a vortex is clearly observed. Flow state (c) was computed at a set of parameters below the curve; the turn around flow does not present a vortex.

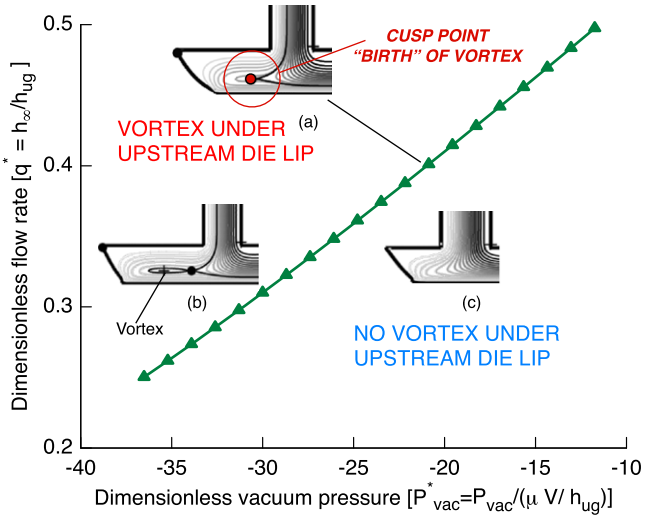


**Fig. 6.** Solution path of the augmented Navier–Stokes system. All the states on the path satisfy the vortex birth condition and, consequently present a cusp point, as indicated in (a)–(c) are streamlines at a set of parameters above and below the computed path.

Vortex appears when the length of the upstream bead is long enough, i.e at high flow rates and high vacuum (more negative) pressure.

With the discretization used here, e.g. 18,300 degree of freedom, each solution of the Navier–Stokes system alone took approximately 60 s in a 1.7 GHz IBM power 4 system (about 6 iterations per solution, ~9.96 s per iteration). The solution of each point along the vortex birth path, i.e. the solution of the Navier–Stokes system augmented by the vortex birth condition: took approximately 220 s in the same machine. (about 20 iterations per solution, ~11.1 s per iteration). The line that defines the flow states at which vortex birth occurs was constructed by using 20 different values of vacuum pressure $P_{vac}$, leading to a total computational time of approximately $20 \times 220$ s = 4400 s. Assuming that in order to find the critical flow rate at each value of vacuum pressure at which a vortex is born from a cusp point, 20 different solutions of the Navier–Stokes are needed, the total cost to predict the vortex-free window by vortex capturing is $20 \times 20 \times 60$ s = 24,000 s. The time required to post-process the solutions is not included in this estimation. The method described in this work is faster by a factor of ≈5.5 even without considering the necessary and tedious user intervention associated with post-processing the computed flow fields. Furthermore, the accuracy of the critical flow states computed by tracking the vortex birth is much higher than what can be obtained by post-processing solutions at different set of flow parameters.

*4.1.2. Tracking onset of separation point at solid wall*

According to Sartor [22], a converging downstream die lip geometry broaden the possible operating ranges of vacuum pressure and coating speed. The converging channel causes the formation of a pressure hill in this part of the flow. This high pressure helps to push the upstream meniscus away from the feed slot enabling thin coating at lower vacuum pressure. However, this adverse pressure gradient can create a flow detachment at the downstream die lip leading to a vortex formation, as illustrated in Fig. 5. The presence of vortex may limit the operating ranges when coating quality is important.

In this study, we focus on the effects of two parameters: flow rate $q$ and downstream die lip angle $\theta$, as shown in Fig. 5. At a set die lip angle, a smaller flow rate leads to a stronger adverse pressure gradient which can cause flow detachment. For direct tracking of vortex birth from the die lip, we choose the downstream die lip angle $\theta$ as the control variable for continuation method, and flow rate $q$ as the auxiliary parameter for augment Navier–Stokes system. Augmented residuals are the conditions for vortex birth at a solid wall, e.g. Eqs. (30), and the additional auxiliary parameter for augment Navier–Stokes system is one the coordinate $x$ for the birth point along the downstream die lip and the flow rate. The remaining flow parameters are the ones listed in Table 2.

The path of solution of the augmented Navier–Stokes system in the plane of dimensionless flow rate $q^* = q/(V_w h_{ug})$ and die lip angle $\theta$ is presented in Fig. 7. All the flow states over the solution path present a degenerate separation point, as shown in insert (a) of the figure. The results show that at a given flow rate there is a critical die lip angle above which a vortex appears. As illustration, flow fields at a set of conditions above (insert b) and below (insert c) the solution path are also presented.The computed path clearly defines the boundary of the vortex-free region of the parameter space.

*4.2. Half-submerged-forward roll coating*

Forward roll coating is a process whereby liquid flows into a narrow gap between two counter rotating rolls before it splits into two layers, one on each of the roll surfaces [11], as sketched in Fig. 8. The flow near the film-splitting zone is

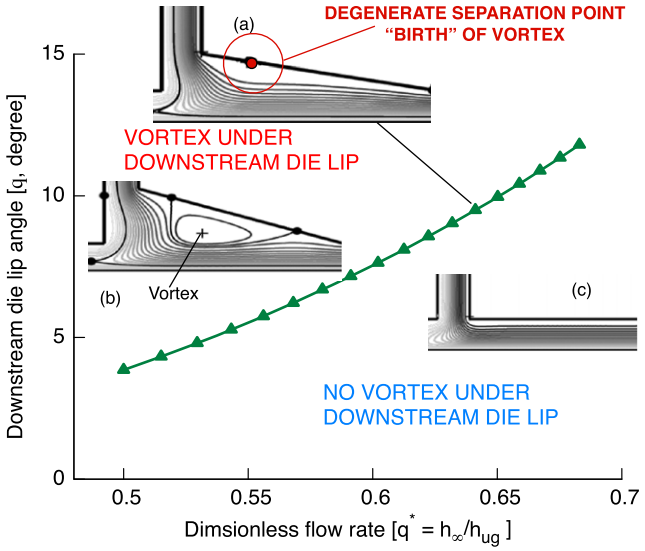


**Fig. 7.** Solution path of the augmented Navier–Stokes system. The computed path marks the boundary of the vortex-free window. The states on the path present a degenerate stagnation point at the wall, as indicated in (a)–(c) are flow states above and below the line.

two-dimensional as shown by [11], and a recirculation may appear depending on operating conditions. We consider the upstream side of the roll submerged into the pool of liquid, so that the flow system has only one meniscus. This prototype forward roll coating is so called *half-submerged-forward roll coating* (HSFR), as discussed by Carvalho [5,7] and Coyle et al. [11].

The complex flow pattern of film-splitting flows between rigid rolls has been extensively studied in the past. Coyle [10] described the flow near the film splitting meniscus using lubrication theory and the full Navier–Stokes equation. He found that at low capillary number and large gaps, a recirculation attached to the meniscus could be observed. He also pointed out that when the symmetry of the flow is broken (the speed ratio is different than one), topological changes in the film-splitting zone is observed: the two vortices attached to the free surface split and one of them moves upstream and is not attached to the meniscus, as illustrated in Fig. 9(c).

Benjamin [2] named them internal gyre and free-surface gyre, and captured the flow state changes with respect to parameters using post-processing. Gaskell et al. [13] analyzed the vortex structures in forward roll coating and their dependence on the operating parameters. The analysis was done by post-processing a series of steady state solutions at different operating parameters. Wilson et al. [26] also examined the evolution of vortex-saddle patterns in both the free surfaces as changing operating parameters.

In this study, we consider a Stokes flow of a HSFR situation and focus on the vortex birth near the film-splitting zone. In order to represent the detail flow structure in this zone, the finite element mesh is designed so that elements are concentrated near the film splitting meniscus, as shown in Fig. 8(b). Boundary conditions are summarized in Fig. 8(a). Table 3 lists the operating parameters considered as the base case. The synthetic inflow and outflow boundaries were located such that the solution was virtually independent of their locations. The values used here were $L_u = 50$ mm and $L_d = 60$ mm.

In this study, we apply the tracking algorithm in both the symmetric flow, e.g. equal roll radii and speed ratio equal to one, and flow with speed ratio different than one. Possible streamline patterns of both cases are presented in Fig. 9(b) and (c).

*4.2.1. Tracking onset of degenerate stagnation point at free surface (symmetric flow)*

In the symmetric flow there is always a stagnation point at the intersection of the free surface, and the symmetry plane, even in the cases where there is no recirculation. This stagnation point gives birth to two vortices simultaneously, as sketched in Fig. 9(b).

The presence of the recirculation attached to the free surface depends on the strength of the adverse pressure gradient that slows down the liquid as it approaches the meniscus and on the location of the free surface.

In this study, we focus on the effects of two parameters on the flow pattern: the half-gap height $H_0$ and the roll angular speed $\Omega^l_{\text{roll}}$. For direct tracking of vortex birth from the free surface, we choose the roll angular speed as control variable for continuation, and the half-gap height as the auxiliary parameter for the augment Navier–Stokes system. Augmented residuals are the conditions for vortex birth attached to a free surface, e.g. Eqs. (28), and the additional auxiliary parameter for augment Navier–Stokes system is the coordinate $y$ of the birth point along the free surface and the half-gap height $H_0$. The remaining flow parameters are listed in Table 3.

**Fig. 8.** Half-submerged-forward roll coating: boundary condition and mesh.

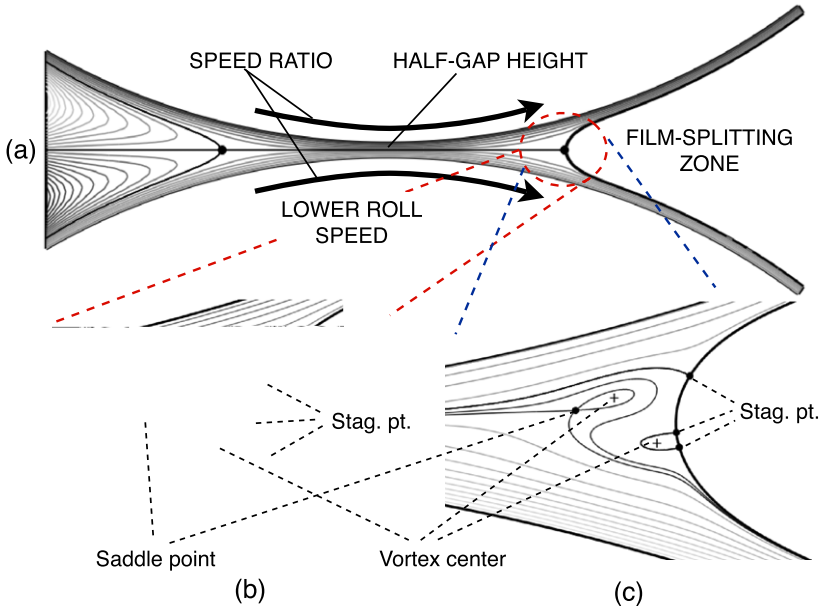


**Fig. 9.** Possible vortex structure in half-submerged forward roll coating and flow parameters which can induce vortex birth. Three figures, (a)–(c), are streamline plots of forward roll coating at different conditions. "Stag. pt." means stagnation point. (a) represent forward roll coating without vortex. When the system is symmetric, i.e. roll speed ratio between upper and lower roll is one, vortex structure is also symmetric as in (b). When the system is asymmetric, i.e. roll speed ratio is not unity, vortex structure loses symmetricity as in (c).

**Table 3**
Parameters used in half-submerged forward roll coating.

| Name | Unit | Base case |
|---|---|---|
| *Operating parameters* | | |
| Upper roll angular speed ($\Omega^u_{\text{roll}}$) | rad/s | 9.5 |
| Lower roll angular speed ($\Omega^l_{\text{roll}}$) | rad/s | 9.5 |
| Ambient pressure ($P_{\text{amb}}$) | Pa | 0 |
| Inflow boundary pressure ($P_{\text{in}}$) | Pa | 0 |
| Surface tension ($\sigma$) | dyne/cm | 58 |
| Viscosity ($\mu$) | MPa · s | 2.3 |
| Half gap height ($H_0$) | mm | 1 |
| Upper roll radius ($R^u$) | mm | 100 |
| Upper roll radius ($R^l$) | mm | 100 |
| Dimensionless variables used in vortex-free window | | |
| Name | | Definition |
| Dimensionless gap height ($H^*_0$) | | $\frac{H_0}{R^l}$ |
| Capillary number ($Ca$) | | $\frac{\mu\Omega^l_{\text{roll}}R^l}{\sigma}$ |
| Speed ratio ($S$) | | $\frac{\Omega^u_{\text{roll}}}{\Omega^l_{\text{roll}}}$ |

Two types of vortex birth occur in the asymmetric flow: the vortex attached to the upstream saddle point comes from a cusp point inside the flow and the vortex attached to the free surface comes from a degenerate stagnation point at the free surface. The conditions at which the vortices appear is not the same. We track the birth of both vortices as a function of the capillary number and speed ratio.

For direct tracking of both vortex births, we choose the speed ratio as the control variable for continuation, and the lower roll angular speed as the auxiliary parameter for the augment Navier–Stokes system. For tracking the vortex birth from the cusp point, the augmented residual are the conditions given by Eqs. (27), and the additional auxiliary parameters for the augment Navier–Stokes system are the two coordinates $x$ and $y$ of the cusp point and the lower roll speed.

For the tracking the vortex birth from the free surface, the augmented residuals are conditions given by Eqs. (28), and the additional auxiliary parameter for the augment Navier–Stokes system is the coordinate $y$ of the degenerate stagnation point

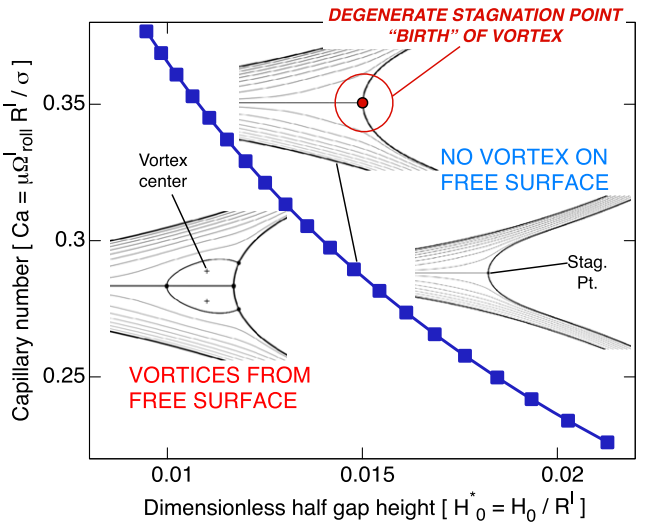


**Fig. 10.** Solution path of the augmented Navier–Stokes system. The computed path marks the boundary of the vortex-free window. The states on the path present a degenerate stagnation point at the meniscus, as indicated in (a). (b) and (c) are flow states above and below the line.

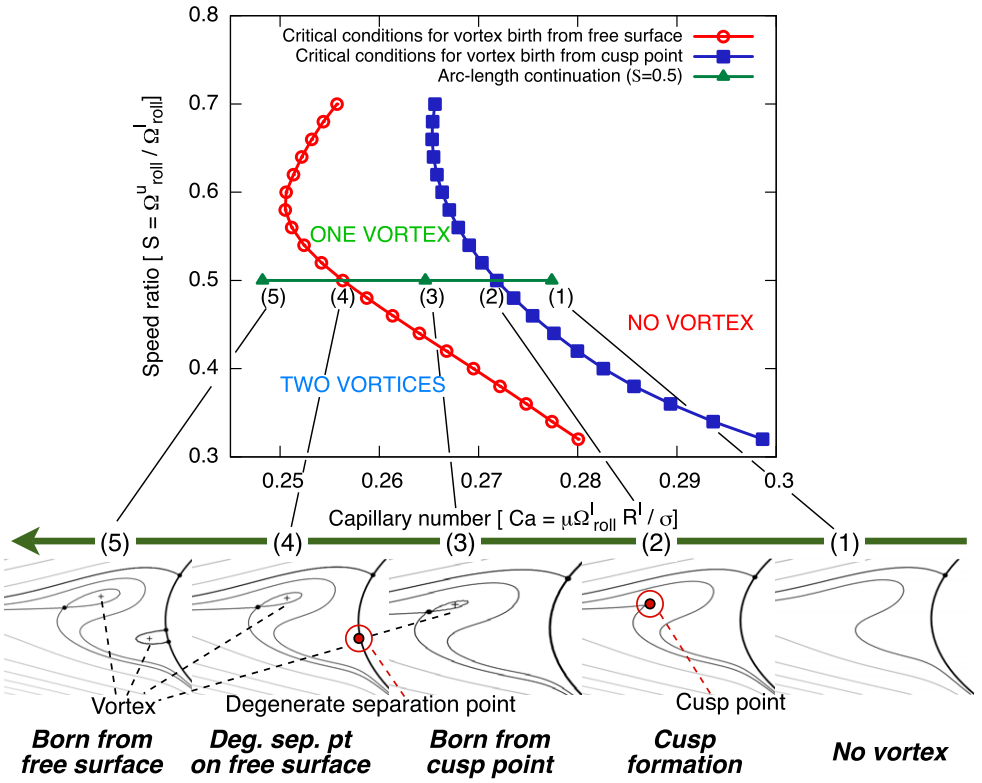


**Fig. 11.** Solution paths of the augmented Navier–Stokes systems for vortex birth from saddle point (squares) and from a free surface (circles). The line define the regions of the parameter space without vortex (insert 1), with a single & vortex inside the flow (insert 3) and with two vortices (insert 5).

along the free surface and the lower roll speed. Both solution paths are presented in Fig. 11. The curve on the right corresponds to the flow states with a cusp point inside the flow, it defines the set of conditions at which a vortex inside the flow

is about to appear, as shown in insert (2). The curve on the left defines the conditions at which a degenerate stagnation point attached to the free surface can be observed, as illustrated in insert (4) of the figure. It defines the set of conditions at which the vortex attached to the meniscus appears. These two solution paths of the corresponding augmented Navier–Stokes system define the boundaries of the vortex-free window, single vortex region and two vortices window.

The evolution of the streamline pattern as the capillary number (lower roll speed) falls is also presented in Fig. 11. At high capillary number, there is no vortex near the free surface. There is only one stagnation point in this region. It is the termination point of the separating streamline that divides the flow towards the upper or lower roll. As the lower roll speed falls, a cusp point is formed leading to a recirculation inside the flow. As the lower roll speed falls further, a degenerate stagnation point is formed on the meniscus, leading to a recirculation attached to the free surface. At low capillary number, there are two vortices near the film splitting meniscus.

## 5. Final remarks

Vortices in flow can cause undesired effects in many industrial processes, especially for continuous liquid coating on moving substrate. It is important to know the region of the operating parameters space at which vortices are not present in the coating flow, so these set of parameters can be avoided during operation. These regions are called vortex-free operating window. In computer-aided analysis and design, the most effective way to construct these is not to check a large set of solutions *a posteriori*, but to delineate the range of design parameters and operating conditions that define the boundary of the vortex-free window. This means tracking the birth (of death) of vortices of three kinds: *free* in the flow, *attached* to solid wall or liquid free surface. A way of doing this is to solve the Navier–Stokes or related governing equations, after augmenting the system with one or more equations that describe the local kinematic conditions at vortex birth and with an equal number of design parameters or operating conditions as new unknowns. Two liquid coating processes – single-layer slot coating and forward roll coating – were chosen as examples of automatic generations of vortex-free windows. In the slot coating, vortex birth under the upstream die lip and under the downstream die lip were tracked to give guidelines of preferred range of flow rate, vacuum pressure and die lip angles. In the roll coating, we focused on the generation of recirculations near film splitting zone. For symmetric flow, we were able to construct the path of multiple vortices birth in the parameter space represented by gap and capillary number. For asymmetric flow with roll speed ratio different from one, the birth of two different vortices near the meniscus were tracked to delineate the boundaries of the vortex-free window, single vortex region and two vortices window in flow topology map.

## Acknowledgments

We are grateful for resources from the University of Minnesota Supercomputing Institute. J.N. and M.S.C. would like to dedicate this work to the late Prof. “Skip” Scriven.

## References

[1] P.G. Bakker, Bifurcations in Flow Patterns, Kluwer Academic Publishers, 1991.
[2] D.F. Benjamin, Roll coating flows and multiple roll systems, Ph.D. Thesis, University of Minnesota, Published by University Microfilms International, Ann Arbor, MI, 1994..
[3] M. Brøns, Topological fluid dynamics of interfacial flows, Phys. Fluids 6 (1994) 2730–2737.
[4] M. Brøns, J.N. Hartnack, Streamline topologies near simple degenerate critical points in two-dimensional flow away from boundaries, Phys. Fluids 11 (1999) 314–324.
[5] M.S. Carvalho, Roll coating flows in rigid and deformable gaps, Ph.D. Thesis, University of Minnesota, Minneapolis, 1996..
[6] M.S. Carvalho, H.S. Kheshgi, Low flow limit in slot coating: theory and experiments, AIChE J. 46 (2000) 1907–1917.
[7] M.S. Carvalho, L.E. Scriven, Three-dimensional stability analysis of free surface flows: application to forward deformable roll coating, J. Comput. Phys. 151 (1999) 534–562.
[8] T.F. Chan, Newton-like pseudo-arclength methods for computing simple turning points, SIAM J. Sci. Stat. Comput. 5 (1984) 135–148.
[9] K.N. Christodoulou, L.E. Scriven, Discretization of viscous free surface flows and other free boundary problems, J. Comput. Phys. 99 (1992) 39–55.
[10] D.J. Coyle, The fluid mechanics of roll coating: steady flows, stability, and rheology, Ph.D. Thesis, University of Minnesota, Minneapolis, 1993..
[11] D.J. Coyle, C.W. Macosko, L.E. Scriven, Film-splitting flows in forward roll coating, J. Fluid Mech. 171 (1986) 539–571.
[12] J.M. de Santos, Two-phase cocurrent downflow through constricted passage, Ph.D. Thesis, University of Minnesota, Minneapolis, 1995..
[13] P.H. Gaskell, M.D. Savage, H.M. Thompson, Stagnation-saddle points and flow patterns in Stokes flow between contra-rotating cylinders, J. Fluid Mech. 370 (1998) 221–247.
[14] I.D. Gates, Slot coating flow: feasibility, quality, Ph.D. Thesis, University of Minnesota, Minneapolis, 1999..
[15] P.M. Gresho, R.L. Sani, Incompressible Flow and the Finite Element Method: Advection–Diffusion and Isothermal Laminar Flow, John Wiley& Sons, 1998.
[16] B.G. Higgins, L.E. Scriven, Capillary pressure and viscous pressure drop set bounds on coating bead operability, Chem. Eng. Sci. 35 (1981) 673.
[17] H. Keller, Numerical solution of bifurcation and nonlinear eigenvalue problems, in: P.H. Rabinowitz (Ed.), Applications of Bifurcation Theory, Academic Press, New York, 1977, pp. 359–384.
[18] S.F. Kistler, L.E. Scriven, Coating flow theory by finite element and asymptotic analysis of the Navier–Stokes system, Int. J. Numer. Methods Fluids 4 (1984) 207–229.
[19] H.J. Lugt, Vortex flow in Nature and Technology, John Wiley & Sons, 1983.
[20] H.J. Lugt, Local flow properties at a viscous free surface, Phys. Fluids 30 (1987) 3647–3652.
[21] L.C. Musson, Two-layer slot coating, Ph.D. Thesis, University of Minnesota, Minneapolis, 2001..
[22] L. Sartor, Slot coating: fluid mechanics and die design, Ph.D. Thesis, University of Minnesota, Minneapolis, 1992..
[23] P.M. Schweizer, Visualization of coating flows, J. Fluid Mech. 193 (1988) 285–302.

[24] R. Seydel, Practical Bifurcation and Stability Analysis, Springer-Verlag, 1994.
[25] M. Vinokur, On one-dimensional stretching functions for finite-difference calculations, J. Comput. Phys. 50 (1983) 215–234.
[26] M.C.T. Wilson, P.H. Gaskell, M.D. Savage, Flow in a double-film-fed fluid bead between contra-rotating rolls Part 1: Equilibrium flow structure, Eur. J. Appl. Math. 12 (2001) 395–411.
[27] A. Yeckel, L.E. Scriven, Multiparameter continuation methods for tracking desired flow states, in: Proceedings of the 1992 ACM/IEEE Conference on Supercomputing, 1992, pp. 142–151.
[28] A. Yeckel, Tools for parameter studies in fluid dynamics, Int. J. Numer. Meth. Fluids 28 (1998) 1199–1216.